Chapter 2

Constraints on Ediacaran carbon cycle dynamics from the Shuram Excursion of Oman

Kristin D. Bergmann[1], John P. Grotzinger[1], Magdalena Osburn[1], John M. Eiler[1], Woodward W. Fischer[1]

[1]California Institute of Technology

2.1 Abstract

Neoproterozoic large negative carbon isotope excursions remain an enigmatic feature of the long-term carbon isotopic record yet their temporal distribution predating the appearance and diversification of complex animals in the fossil record demands an improved understanding of them. There is considerable uncertainty on whether these extreme excursions reflect primary perturbations in marine DIC [1, 2, 3], or whether they are post-depositional features [4, 5, 6, 7]. We examine problematic aspects of the largest negative excursion on record—the Shuram Excursion in the Sultanate of Oman including: (1) co-variation in δ^{13}C and δ^{18}O carbonate, (2) elevated trace metal signatures, and (3) isotopic variability between the different carbonate phases [2, 7, 6, 5]. We combine bulk and micro-scale analysis

of isotopic composition using carbonate clumped isotope thermometry and SIMS, and trace metal enrichments using ICP-OES, XANES and electron microprobe measurements. We find there is little evidence for large-scale isotopic re-ordering associated with open-system diagenesis [5, 6, 8], instead the bulk of the $\delta^{18}O_{min}$ trend can be explained by a two-step change in depositional conditions caused by 1) a temperature increase and fluid composition change from enriched evaporative fluids to open marine fluids and 2) a mineralogical shift from dolomite to calcite. The excursion is correlated with an increase in fine-grained, poorly weathered detrital material that accounts for the majority of the increase in bulk trace metal enrichment. The results of this study suggest these rocks preserve their primary isotopic character and the extreme depletion reflects a secular change in marine DIC, which supports previous hypotheses that this important event may have had a critical role in the appearance of Ediacaran fauna [1, 9].

2.2 Introduction

The extreme variability of the Neoproterozoic carbon isotopic record has received much attention of late (e.g., [2, 7, 10, 6]). The record is characterized by a positive baseline of $\sim +5$ that is punctuated by large negative excursions [11]. The most extreme negative excursion on record, the so-called Shuram Excursion, was first discovered in the Shuram Formation of the Nafun Group of Oman and has been since documented in many other Ediacaran-aged successions including South Australia, South China, Western USA and likely also in Siberia, Scandinavia, Scotland and Namibia [12, 1, 13, 14, 15, 16, 17, 18, 19, 20, 21]. The carbonate isotopic composition reaches $\delta^{13}C_{VPDB}$ values of -12‰ in the nadir of the excursion and remains at extreme negative values for hundreds of meters of shelf stratigraphy [12, 1, 13, 14, 15]. While no direct geochronological constraints exist on the strata that record such extreme $\delta^{13}C$ values, they are constrained to between 600-551 Ma, post-dating the Marinoan Glaciation and pre-dating the Precambrian-Cambrian Boundary [22, 2, 20]. In both South Australia and the Western USA, the negative excursion is stratigraphically below the first appearance of Ediacaran fauna [23, 13, 24].

The lowest of these negative isotopic values are problematic because they sit outside of the traditional solution space of the steady-state carbon isotope mass balance model used to understand long-term carbon isotopic variation (e.g., [25]). These negative values are more negative that the assumed δ^{13}C input composition from weathering and volcanic outgassing of $\sim$ -6‰Ṫwo distinct classes of hypotheses have been put forward to explain these global negative excursions. The first class proposes the carbon isotopic system during this interval of Earth's history cannot be understood with traditional assumptions made in the isotopic mass balance model. Mechanisms within this class include two dynamic reservoirs where the dissolved organic carbon (DOC) reservoir dramatically changed size over the coarse of the excursion [3, 1], the system was operating at quasi-steady state [3], there was a significant change in the isotopic composition of the inputs [26]. A recently proposed model alters the carbon isotope mass balance model from a two sink to three sink model [7], postulating the Neoproterozoic large negative excursions are composed of a significant amount of authigenic depleted δ^{13}C carbonate that formed in the sediments. The second class of hypotheses regarding the extreme negative carbon isotopic excursions suggest they have no direct connection to dynamics within the marine carbon cycle because they are not a primary feature [4, 5, 6]. These authors have pointed to aspects of the strata preserving these excursions that they argue suggest diagenetic processes have altered the δ^{13}C values including: (1) co-variation in δ^{13}C and δ^{18}O carbonate, (2) elevated trace metal signatures, and (3) a lack of co-variation in $\delta^{13}C_{carb}$ and $\delta^{13}C_{org}$ [6, 5].

Central to the debate on whether these excursions are recording time-varying behavior in marine DIC is the striking correlation between δ^{13}C and δ^{18}O of the carbonate. This correlation is not expected from most primary processes because of the different residence times of carbon and oxygen in the global ocean and the largely uncoupled nature of the two isotopic systems. Co-variation has been observed via open-system diagenesis in younger rocks where large pore volumes of

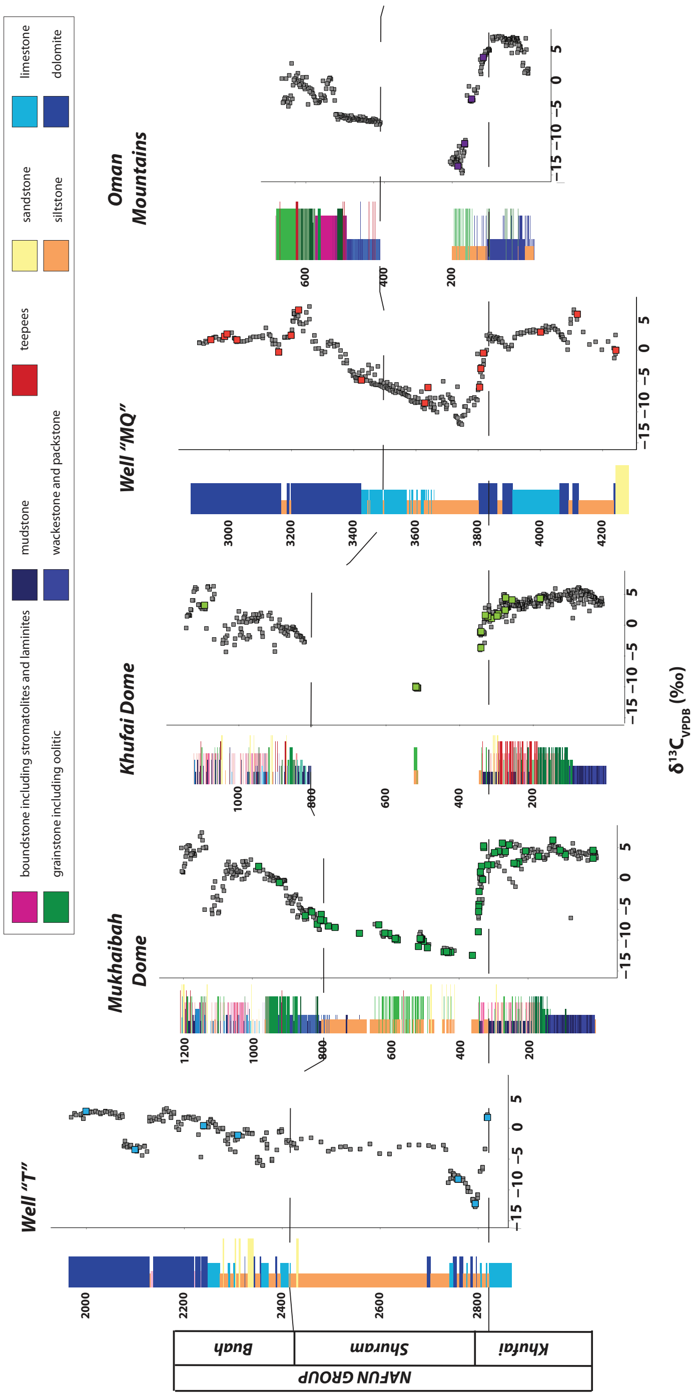

Figure 2.1: δ^{13}C and lithofacies of the five sections analyzed. Wells 'TM6' and 'MQ1' are plotted versus their current burial depth whereas 'MD' 'KD' and 'MTN' are plotted versus stratigraphic height. The sections are aligned on the onset of the Shuram Excursion which corresponds to a sequence boundary in the outcrop sections 'MD' and 'KD'.

Grey data and outcrop stratigraphy from this study (Shuram and Buah fms.) and [27] (Khufai Fm.) and grey data for MQ1 and TM6 from [28]

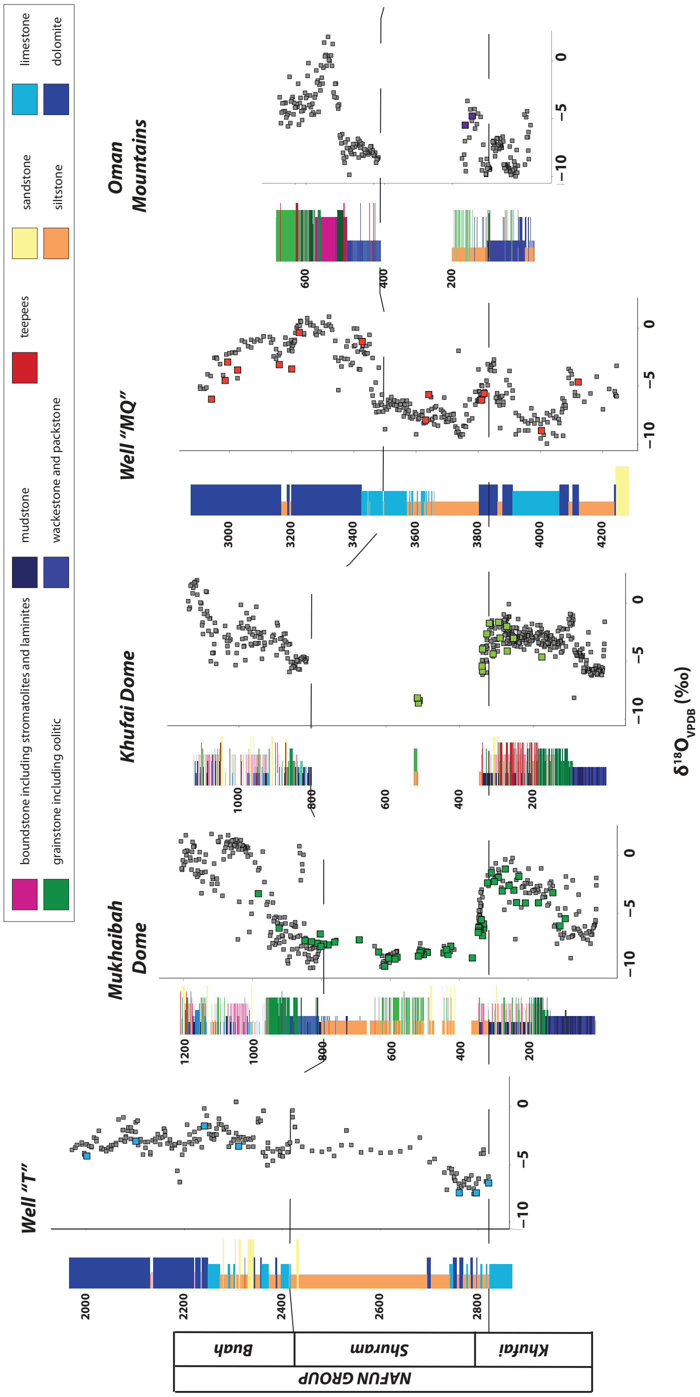

Figure 2.2: $\delta^{18}O_{min}$ of the five sections analyzed. Wells 'TM6' and 'MQ1' are plotted versus their current burial depth whereas 'MD' 'KD' and 'MTN' are plotted versus stratigraphic height. The sections are aligned on the onset of the Shuram Excursion which corresponds to a sequence boundary in the outcrop sections 'MD' and 'KD'.

Grey data and outcrop stratigraphy from this study (Shuram and Buah fms.) and [27] (Khufai Fm.) and grey data for MQ1 and TM6 from [28]

^{13}C-depleted fluids flush through a package of rocks creating a diagenetic array of successively altered carbonates [8, 29, 30]. The co-variation between δ^{13}C and δ^{18}O of the carbonates recording the excursion has produced two different post-depositional diagenetic models for extreme negative carbon isotope excursions, a burial model where the carbonates have been flushed with isotopically depleted δ^{13}C hot basinal brines [5], and a meteoric model where the carbonates have been flushed with isotopically depleted terrestrial δ^{13}C and isotopically depleted meteoric fluids [6]. However, it is important to remember there are documented Phanerozoic examples that exhibit a primary correlation between δ^{13}C and δ^{18}O where these excursions have known climatic forcing (i.e., the PETM and end-Ordovician glaciation) but the isotopic range is smaller (-1.5‰ in δ^{18}O for the PETM; +5‰ in δ^{18}O for the end-Ordovician glaciation) [31, 32].

If the Shuram excursion is caused by a post-depositional diagenetic process, its temporal significance precceeding the rise of Ediacaran fauna and the diversification of animals would have no implications for the environmental conditions and oxygen budget leading into these significant evolutionary events [33, 23]. Importantly, if the small-scale differences in the δ^{13}C isotopic composition of successive carbonate strata that researchers currently interpret as 'excursions' can be produced by post-depositional processes like recrystallization and precipitation of secondary phases, this would call into question the long-term validity of the carbon isotopic record as a whole. Current interpretations tying the δ^{13}C isotopic record to the historic behavior of the carbon cycle and indirect links to the oxygen budget would prove questionable. Additionally, prior to rise of animals, the carbon isotopic composition of individual stratigraphic sections are currently used for correlation purposes to other sections globally, a practice that may be partially invalidated if such records are significantly modified during burial.

The ongoing debate about whether these excursions have implications for the dynamics of the Neoproterozoic carbon cycle and oxygen budget led us to use a combined approach of bulk and micro-scale techniques to constrain the diagenetic history of the rocks recording the Ediacaran Shuram excursion in the Sultanate of Oman [12, 34]. The three models proposing that these extreme negative excursions are caused by large-scale recrystallization of the carbonates in the presence of exotic fluids [6, 5] or represent the formation of volumetrically significant amounts of δ^{13}C depleted authigenic carbonates [7] make specific predictions for the sedimentary character, petrography, micro-scale geochemistry and clumped isotope geochemistry of these rocks. Specifically, we will present results from (1) carbonate 'clumped' isotope thermometry which can independently determine the precipitation temperature of both calcite and dolomite. Using traditional δ^{18}O paleothermometry [35, 36], the precipitating fluid composition can be solved for (i.e., marine, meteoric, or hot basinal brine), thus the diagenetic mechanisms proposed for large negative carbon isotope excursions that require flushing with exotic fluids to create a correlated array in δ^{13}C and δ^{18}O are directly testable [5, 37, 6, 38] (2) micro-scale analysis using secondary ion mass spectrometry (SIMS) that can measure the isotopic composition of primary vs. authigenic carbonate phases testing the importance of a volumetrically significant authigenic carbonate phase during these excursions [7] and (3) micro-scale elemental analysis using the electron microprobe which can identify the specific components that result in elevated bulk trace metal compositions.

2.3 Geologic Setting

The Shuram Excursion is recorded in the strata of the Khufai, Shuram and Buah Formations within the Ediacaran- to Cambrian-aged Huqf Supergroup (Fig. 2.7, Fig. 2.1) [39, 2, 40]. In central Oman, the Khufai Formation is composed of shallow-water carbonates deposited on a carbonate ramp. In general the carbonates in the Huqf show a generalized upwards shallowing of the lithofacies and lateral progradation. The Lower Khufai Formation is composed of medium to thick intraclast wackestone event beds deposited below storm weather wave base [41]. In contrast, the Middle and Upper Khufai Formation was deposited in a peritidal environment with minimal accommodation space, restriction and evaporation. These rocks have undergone almost complete early, fabric-preserving dolomitization [41]. Lithofacies include cross-bedded oncolite grainstone, tufted laminite, domal stromatolites, intraclast conglomerate and structures including teepees associated with evaporite mineral pseudomorphs and brecciation (Fig. 2.3c) [41]. The most proximal facies in the Upper Khufai Formation (i.e., teepees and breccia) are overlain by aggradding stromatolites and oolitic grainstone indicating a sequence boundary exists where the depositional environment changes from one dominated by exposure to one characterized by slow flooding and increased accommodation space [41]. The carbonate strata above the sequence boundary preserve the initial decline in δ^{13}C and δ^{18}O of the Shuram Excursion. The dolomitic lithofacies of the uppermost Khufai, including stromatolites and cross-stratified ooid grainstone can preserve $\delta^{13}C_{VPDB}$ compositions as depleted as -8.5‰ (Fig. 2.6). One would predict a transition from a restricted evaporative environment to a flooded platform in connection with open marine water would have a isotopic change in the fluid composition. The maximal transgression and flooding is coincident with the introduction of thick red siltstone deposits and a loss of carbonate lithofacies marking the start of the siliciclastic dominated Shuram Formation (Fig. 2.3d) [34, 41]. The middle and upper Shuram Formation is better exposed in outcrop and consists of repeated parasequences of hummocky cross-stratified siltstone capped by trough to planar cross-stratified limestone ooid grainstone with $\delta^{13}C_{VPDB}$ isotopic compositions as low as -12‰ (Fig. 2.3d) [40, 34]. The siltstone contains evidence for soft sediment deformation including ball and pillow structures [40]. The recovery of the Shuram excursion occurs in the lower Buah Formation, which is also composed of shallow-water carbonates that indicate a general upwards shallowing of the lithofacies. The lowermost Buah is composed of limestone crinkly laminite and edgewise conglomerate, a lithofacies interpreted as a partially lithified seafloor that is reworked and stacked on edge by oscillatory wave action. (Fig. 2.3f) [42]. This reworking of the seafloor potentially occurred during storm events. The gradual isotopic recovery continues above a sequence boundary that shows a rapid increase in accommodation space, a shutoff in the siliciclastic input and the aggradation of

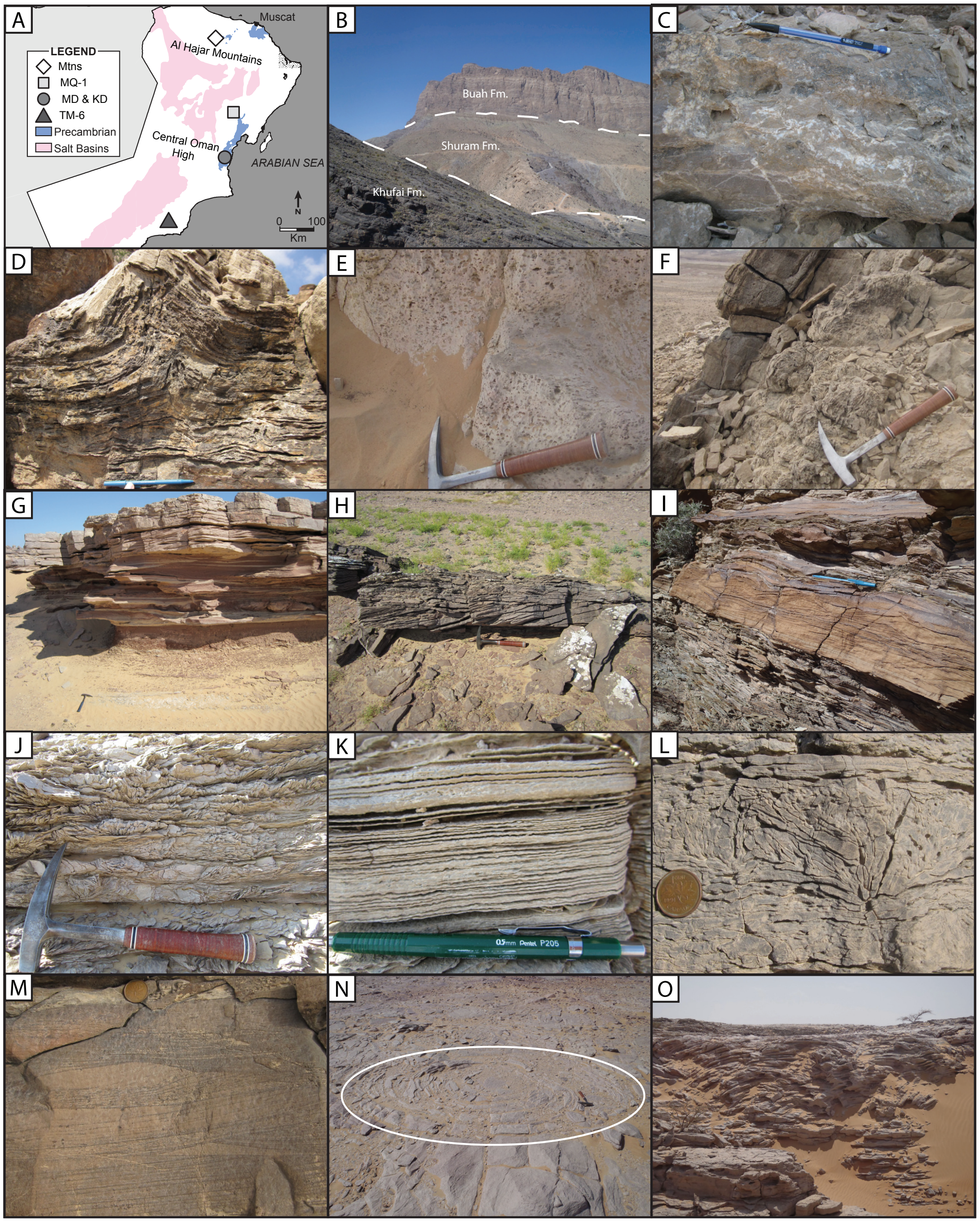

Figure 2.3: Geologic context of the Shuram excursion. A) Location map of the five stratigraphic sections analyzed. B) Diagenetic calcite from the Lower Khufai Formation C) Peritidal deposits of the Upper Khufai D) Transgressive deposits recording the onset of the negative excursion in the Upper Khufai E) Siltstone capped by ooid grainstone in the middle Shuram Formation F) Climbing ripples in the Shuram Formation from the Oman Mountains G) Edgewise conglomerate and crinkly laminite from the lower Buah Formation.

large reefal stromatolite mounds filled in with trough cross-stratified grainstone shoals (Fig. 2.7, Fig. 2.1).

In the Oman Mountains the Khufai Formation is thinner, completely limestone and is predominantly intraclast wackestone and mudstone deposited as turbidites below storm weather wave base. The Upper Khufai Formation is marked by successive large-scale (3 m) slump beds and in a few locations including Wadi Bani Awf significant coarse grained sandstone beds [34, 41]. The Shuram Formation is dominantly composed of siltstones alternating with ripple-stratified silty carbonate grainstone beds with gutter casts on bed bottoms. The ripples indicate significant aggradation during ripple formation producing asymmetrical climbing wave ripple morphologies (Fig. 2.3e) [34]. The Buah Formation has a broadly similar lithofacies progression to the Huqf outcrop area with more significant lithofacies differences between Wadi Hajir and Wadi Bani Awf, the latter being more distal [43, 44].

To constrain the importance of post-depositional diagenetic processes on the carbon isotope excursion, samples were analyzed from five stratigraphic sections including two from subsurface drill cores (current burial depths TM6: 2200–2900 m and MQ1: 3300–3900 m, respectively) [12, 1], two from shallowly buried strata from the Huqf outcrop area (MD & KD < 2 km max burial depth), and one from deeply buried strata from the Oman Mountains (MTN > 7 km max burial depth) (Fig. 2.3a, Fig. 2.7). All carbonate samples analyzed in this study from the outcrop locations were composed of $> 70\%$ primary grains or micrite and $< 30\%$ post depositional diagenetic cements. All five sections preserve the striking negative excursion, where $\delta^{13}\mathrm{C}_{VPDB}$ values fall rapidly to values of -12‰ and have a corresponding negative excursion in δ^{18}O (Fig. 2.1, Fig. 2.2) [12]. The similarity in δ^{13}C composition across all sections indicate the excursion was recorded early in these rock's history and is not affected by their widely different burial histories (< 2 km to > 7 km). The Oman Mountains section shows anomalous extreme δ^{18}O depletion which supports the long-held understanding that deep burial can significantly alter the δ^{18}O of carbonates(Fig. 2.2) [12].

2.4 Methods

2.4.1 Sample collection and preparation

Carbonate samples were collected from outcrop locations from the Huqf Outcrop area and Oman Mountains in the winters of 2010 and 2011. Stratigraphic sections were measured and sampled in stratigraphic height at Mukhaibah Dome (MD), Khufai Dome (KD) in the Huqf Outcrop area and at Wadi Sahtan and Wadi Hajir in the Oman Mountains (MTN) [41]. Hand samples were cut to expose an unweathered face prior to further analysis. A variety of lithofacies were analyzed from each stratigraphic section including mudstone, stromatolite boundstone, oolitic grainstone, siltstone, sandstone and edgewise conglomerate and features like teepees [41]. The textural range sampled was in part driven by necessity because no single facies persists through the entire excursion at high resolution. The added benefit of analyzing a range of carbonate facies is an improved understanding of preservation biases associated with specific carbonate textures and different primary porosities that lead to varying contributions from secondary cements.

2.4.2 Carbonate clumped isotope thermometry

Samples were analyzed over the period of Jan, 2009-Jan, 2013. Samples were either drilled from a thin-section billet or from a cut slab with a 3 mm rotary drill bit. Rock cuttings were rinsed to remove drilling mud, dried and powdered in a mortar and pestle. 9–12 mg of powder was weighed into silver capsules before being reacted at 90°C in 100% H_3PO_4 in a common acid bath. Evolved CO_2 was purified by multiple cryogenic traps including a Porapak-Q chromatograph held at -20°C before being measured on a ThermoFinnigan MAT 253 IRMS. Methods for the measurement and corrections to analyzed heated gases run during each session following [45, 46]. After corrections based on the heated gas line from a given session and an intercept shift based on the initial calibration experiment, Δ_{47} values were transformed into an absolute reference frame using a secondary transfer function following [47, 48]. The secondary transfer function for each week was calculated using any of the following available data: 25°C and 1000°C CO_2 as well as any of four carbonate standards with known absolute reference frame values (see below). Finally Δ_{47} values for carbonate samples were corrected by +0.092‰ for the 90°C acid bath reaction temperature within the absolute reference frame [48].

Values within the absolute reference frame (ARF) for two internal standards used over the course of the analyses, Yale CM (n=35) and TV01 (n=50) were calculated from 7 weeks when 1000°C CO_2 was analyzed daily and 25°C CO_2 gases were analyzed bi-weekly. The calculated values for the two standards in the absolute reference frame are reported with 1 SD for all sessions with heated gases and equilibrated gases: Yale CM (n = 33) Δ_{47}-ARF = 0.404 ± 0.022‰, TV01 (n = 50) Δ_{47}-ARF = 0.730 ± 0.018‰. Absolute reference frame values for two other internal standards run during the analytical period were calculated from weeks where either Yale CM and/or TV01 had been run with them (GC-AZ-01 (n=12) and Carmel Chalk (n=15)). Values are reported with 1 SD for all sessions with heated gases and known standards: 102-GC-AZ01 (n = 12) Δ_{47}-ARF = 0.709 ± 0.023‰, and Carmel Chalk (n=15) Δ_{47}-ARF = 0.678 ± 0.020‰. The values of the Carrara standard and 102-GC-AZ01 in the absolute reference frame are nearly identical to those found at Johns Hopkins (UU Carrara (n = 93) Δ_{47}-ARF = 0.403 ± 0.015‰ and 102-GC-AZ01 (n = 102) Δ_{47}-ARF = 0.710 ± 0.015‰ [48].

The reproducibility of standards for all analytical weeks are reported with 1 SD for all sessions: Yale CM (n = 98) Δ_{47}-ARF = 0.405 ± 0.019‰, 102-GC-AZ01 (n = 23) Δ_{47}-ARF 0.710 ± 0.011‰, TV01 (n = 86) Δ_{47}-ARF 0.730 ± 0.015‰ and Carmel Chalk (n = 17) Δ_{47}-ARF 0.675 ± 0.015‰. For single unknown measurements the uncertainty of the measurement is reported as the standard error of the mean (SEM) of Δ_{47} measurements over 8 acquisitions. For $n \geq 2$, the error is reported as the SEM of Δ_{47} over the number of sample replicates.

Temperatures were calculated in the absolute reference frame as well as the interlab reference frame using the same calibration data from two calibration studies completed at Caltech [49, 50]. To build this calibration equation from low to high temperatures we assume that calcite and dolomite calibrations are equivalent. The two approaches do not yield the exact same temperature on a week to week basis and this is likely due to two factors: 1) conversion of the two calibration studies into the absolute reference frame is imperfect because the samples were analyzed before 25°C CO_2 gases were analyzed regularly and 2) Converting unknown samples into the absolute reference frame using both gases and carbonate standards in the transfer function will correct for standard residuals for a given week.

The mineralogy of each powder analyzed was determined by XRD analysis (see below) to properly calculate the $\delta^{18}O_{min}$ composition using unique 90°C acid digestion fractionation factors for calcite and dolomite [51, 52]. Fluid compositions were calculated using the measured clumped isotope temperatures and separate equilibrium fractionation equations for calcite-water [35] and for dolomite-water [36]. For samples that contained mixtures of calcite and dolomite, the dominant mineralogy was used to calculate $\delta^{18}O_{min}$ and $\delta^{18}O_{water}$. Three different dolomite-water equilibrium fractionation equations were compared [53, 54, 36]. Both [36] and [53] produced $\delta^{18}O_{water}$ results in agreement with co-occurring calcite measurements lending faith in the results. The temperature range of dolomite formation from [36] most closely matched the measured temperature range so it was used to calculate the reported water compositions.

2.4.3 Secondary ion mass spectrometry (SIMS)

In situ analysis of $\delta^{13}C$ and $\delta^{18}O$ SIMS analysis was conducted on a Cameca 7f-GEO in the Center for Microanalysis at the California Institute of Technology. The Cameca 7f-GEO was run at a mass resolving power for C of 3000 and for O of 1800. Two thick sections of samples from the nadir of the excursion from the Mukhaibah Dome (MD) and Khufai Dome (KD) sections were imbedded with in-house carbonate standards prior to polishing (Fig. 2.12). A 10 kV Cs^+ beam was held 0.4 nA for C analyses and 1.1 nA for O analyses for spot sizes of 30 μm and 40 μm, respectively. Each spot was pre-sputtered for 120 s. Oxygen was measured on a double Faraday cup system for a count time of 0.96 s for ^{16}O and 4.96 s for ^{18}O using a fast mass peak switching system. Carbon was measured on a single EM with a count time of 0.96 s for ^{12}C and 10.0 s for ^{13}C. A dead time correction was applied to carbon measurements. Secondary ions were collected at -9 kV. 10 measurements of sample unknowns were bracketed with 4 standard analyses on either side. Standard precision was better than 1‰ for δ^{13}C and δ^{18}O for each of the 8 standard analyses bracketing sets of unknowns.

2.4.4 SEM/electron microprobe

A ZEISS 1550 VP Field Emission Scanning Electron Microscope (SEM) equipped with an Oxford INCA Energy 300 X-ray Energy Dispersive Spectrometer (EDS) system within the California Institute of Technology Geological and Planetary Sciences Division Analytical Facility was used for high-resolution imaging of each sample. Images were collected at a working distance between 7-9 mm using a Quadrant Back Scattering Detector (QBSD). In addition EDS spectroscopy measurements of individual minerals were made to identify the types of detrital minerals present in a given sample.

Quantitative elemental spot analysis and elemental mapping on the various carbonate components to assess trace metal variability between textures was conducted on the JEOL JXA-8200 Electron Microprobe. For all quantitative results, the accelerating voltage was 15 kV, the beam current was 20 nA, and the beam size was 1 μm. The CITZAF method was used for matrix correction. Sample standards for the five chemical elements analyzed, included: calcite for Ca, dolomite for Mg, siderite for Fe, rhodochrosite for Mn, strontianite for Sr, and anhydrite for S. Ca had an average detection limit of 177 ppm, Mg–283 ppm, Fe–323 ppm, Mn–300 ppm, Sr–589 ppm, and S–104 ppm.

2.4.5 Carbonate carbon and oxygen isotopic analysis

In addition to the clumped isotope measurements described above, the majority of the higher resolution δ^{13}C and δ^{18}O data was analyzed at the California Institute of Technology on a ThermoFinnigan Delta V Plus attached to a ThermoFinnigan GasBench II. For the samples analyzed at Caltech, approximately 300 μg of carbonate were weighed into gas vials, flushed with UHP He for 5 minutes and reacted with 100% H_3PO_4 at 78°C for 1 hour within the ThermoFinnigan GasBench II. Three standards were run at the beginning of an 88 sample run and then 8 unknown samples were bracketed by 1 standard. Standard reproducibility was better than 0.2‰ in δ^{13}C and better than 0.35‰ and 0.5‰ for δ^{18}O for two in-house standards. Additional samples were analyzed at the University of California, Riverside and University of Nevada, Las Vegas using a similar ThermoFinnigan GasBench setup.

Samples analyzed at the University of Michigan weighing a minimum of 10 μg were placed in stainless steel boats. Samples were roasted at 200°C in vacuo for one hour to remove volatile contaminants and water. Samples were then placed in individual borosilicate reaction vessels and reacted at 77° ± 1°C with 4 drops of anhydrous phosphoric acid for 8 minutes (a total of 12 minutes for dolomites, 17 minutes for apatite, and 22 minutes for siderites) in a ThermoFinnigan MAT Kiel IV preparation device coupled directly to the inlet of a ThermoFinnigan MAT 253 triple collector IRMS. ^{17}O corrected data are corrected for acid fractionation and source mixing by calibration to a best-fit regression line defined by two NBS standards, NBS 18 and NBS 19. Data are reported in ‰ notation relative to VPDB. Precision and accuracy of data are monitored through daily analysis of a variety of powdered carbonate standards. At least four standards are reacted and analyzed daily. Measured precision is maintained at better than 0.1‰ for both carbon and oxygen isotope compositions.

2.4.6 Bulk powder inductively coupled plasma optical emission spectroscopy (ICP-OES)

Bulk ICP measurements were completed at Actlabs and at the Jet Propulsion Laboratory (JPL) on splits of the same drilled powder. The Actlabs method digested up to 0.5 g of sample with aqua regia (HCl + NO_3) for 2 hours at 95°C. Partial reactions are possible for some silicates with this dissolution method. Samples were then analyzed using a Varian ICP-OES for 35 elements.

To target only the bulk limestone between 10 and 80 mg of material was digested in 10% acetic acid for 24 hours at 25°C at the California Institute of Technology. Samples were then filtered to remove particulate oxides and diluted with HCl to minimize introduction issues with the Ar plasma source. Samples were analyzed at the Jet Propulsion Laboratory using a Thermo iCAP 6300 radial view ICP-OES with a Cetac ASX 260 autosampler with solutions aspirated to the Ar plasma using a peristaltic pump. Three standard solutions of 0.5 ppm. 5 ppm and 50 ppm of Mn, Al, Ca, K, Mg, S, Fe and Na, and three standard solutions of 0.1 ppm, 1 ppm and 10 ppm Sr in an acetic-HCl solution to matrix match were run between every 8 sample unknowns.

2.4.7 Bulk powder x-ray absorption near edge spectroscopy

X-ray absorption near-edge spectroscopy (XANES) was conducted at the Stanford Synchrotron Radiation Lightsource (SSRL) on beam line 4-1 on five representative bulk powdered samples from the Shuram Formation in Central Oman. Samples were powdered using a 3 mm rotary drill bit. The powdered samples were spread in a monolayer over Scotch tape and then covered with a second layer of Scotch tape. Approximately 8–16 Scotch tape layers were used for each sample. We used a silicon 220 $\Phi = 90$ crystal and x-ray absorption spectra (XAS) were collected on a Ge multi-element detector for fluorescence and on an absorption detector for transmission spectra. A collimating mirror was used to reduce beam harmonics. XANES spectra of both Fe and Mn spectra were generated for each sample with a scan from 6310–7502 eV. Samples were then normalized for each element and compared to XANES spectra of known standards analyzed under similar conditions.

2.4.8 Bulk powder x-ray diffraction (XRD)

XRD measurements were made on each powder used for clumped isotope measurements on a PANalytical X'Pert Pro within the Material Science at the California

Institute of Technology. Scans were run from 5–70° 2θ with a step size of 0.008 and a scan step time of 10.16 s. A Cu anode was used at 45 kV and 40 mA. A zero-background silicon plate was used for all measurements because of sample size limitations. Mineralogical phases were initially identified using the X'Pert High-score IDMin function. To determine relative abundances of calcite and dolomite in each sample, the relative peak height intensities of the major calcite and dolomite peaks at 29.5° 2θ and 30.7° 2θ, respectively, were used [55]. Mixtures of known compositions of 100%, 80%, 60%, 40%, 20% and 0% calcite with dolomite were used to create the following relationship of peak height to % dolomite for the PANalytical X'Pert Pro setup at Caltech:

$$PercentDolomite = \frac{\frac{Rel.IntensityofCaMgCO_3}{Rel.IntensityofCaMgCO_3+CaCO_3} - 0.0526}{0.0099} \tag{2.1}$$

90% of the samples analyzed were pure end-members of either calcite or dolomite. For the 10% of samples that were a mixture of both calcite and dolomite, the acid digestion fractionation for $\delta^{18}O_{min}$ and min-water fractionation factor for all mixtures in the clumped isotope calculations were made assuming 100% composition of the dominant mineralogy. This will introduce a systematic bias for those samples but most are more than 70% one mineralogy. Another approach would be to use the measured CO_2 gas, and use a weighted average to calculate each portion separately. That approach assumes the two phases have the same $\delta^{18}O$ CO_2 gas composition.

2.5 Results

2.5.1 Carbonate clumped isotope thermometry

The results from the four sections with minimal burial histories (TM6, MD, KD, and MQ1) show similar stratigraphic trends (Fig. 2.4). The $\delta^{13}C$, $\delta^{18}O$ and clumped isotopic character (Δ_{47}) of the Khufai, Shuram and Buah formations are best defined by four stratigraphic divisions: (1) the Lower Khufai Formation,

(2) the Middle and Upper Khufai Formation, (3) the uppermost dolomites of the Khufai Formation recording the onset of the excursion above the sequence boundary, and (4) the nadir and recovery of the excursion in limestones of the Shuram and Buah formations (Fig. 2.4, Fig. 2.2, Fig. 2.6).

The Khufai Formation prior to the onset of the excursion provides an opportunity to examine the clumped isotope temperature range and diagenetic trends in a package of rocks with the same burial history but no δ^{13}C isotopic depletion. There are three types of diagenesis evident in the Khufai Formation: Type 1—high water-to-rock ratio diagenesis of the type suggested to drive the Shuram excursion [5, 6]. Rocks experiencing this type of diagenesis show no change in the fluid composition despite precipitation at higher temperatures suggesting the fluid is abundant and has not evolved due to water-rock interactions where the enriched δ^{18}O of the carbonate rock can enrich small volumes of fluid during exchange. The change in $\delta^{18}O_{min}$ is due to recrystallization at higher temperatures, Type 2—low water-to-rock ratio diagenesis during burial at elevated temperatures. Rocks experiencing Type 2 diagenesis show significant fluid evolution as the small pore volumes become increasing enriched by the water-rock interactions, no change in $\delta^{18}O_{min}$ and precipitation at elevated temperatures, and Type 3—minimal isotopic alteration during lithification preserving near primary, shallow burial temperatures and unmodified fluid compositions (Fig. 2.6). Type 1 diagenesis (high water/rock) is only evident in the Lower Khufai Formation. The carbonates demonstrating this type of diagenesis are significantly recrystallized and are often macroscopically crystalline and penetrated by calcite veins. The clumped isotope temperatures are elevated but fluid compositions remain near 0‰ (T = 45-77°C, avg. $\delta^{18}O_{water}$ = 0.7‰ VSMOW) (Fig. 2.3b, Fig. 2.6). The peritidal carbonates of the Upper Khufai Formation show both Type 2 and Type 3 diagenesis. Samples showing Type 2 diagenesis (low water/rock) are not homogenous and likely contain a component of secondary cement precipitated during burial at elevated temperatures from evolved pore volumes (T = 55-80°C, avg. $\delta^{18}O_{water}$ = 4‰ VSMOW) (Fig. 2.6). Samples indicating Type 3 diagenesis are well preserved petrographically and include

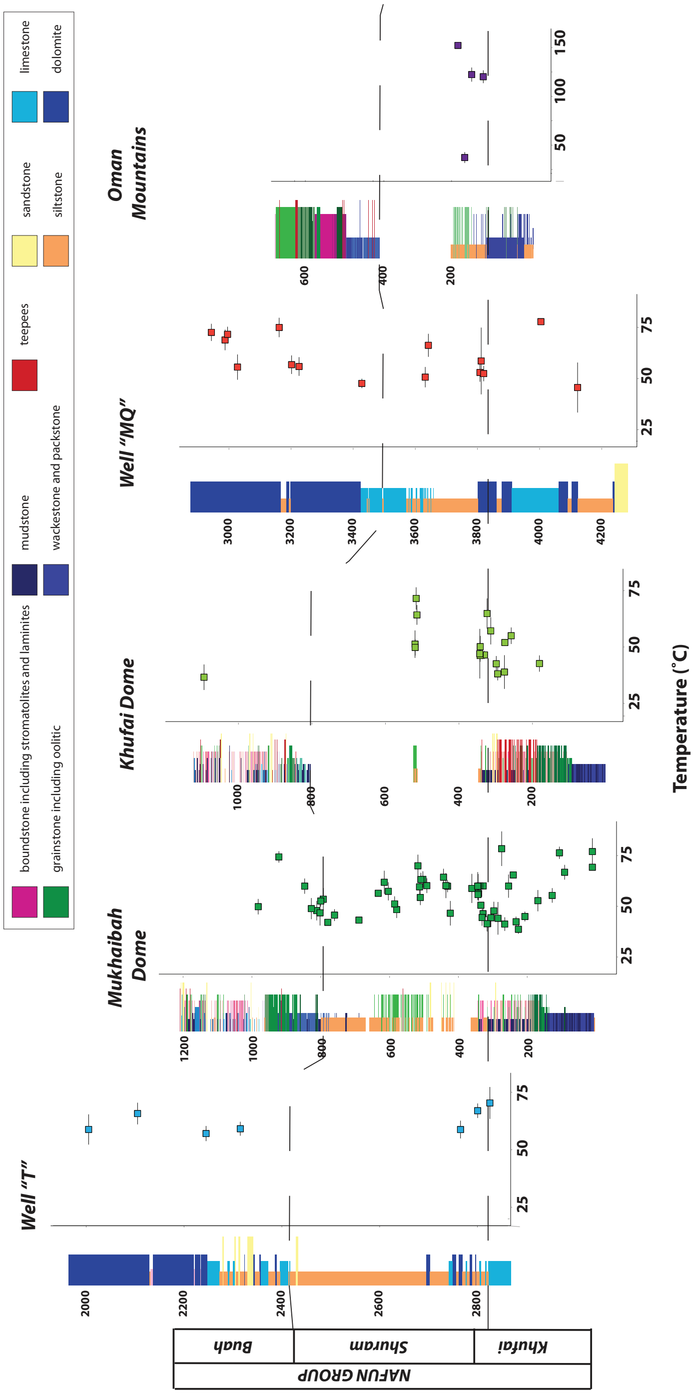

Figure 2.4: Clumped isotope temperature of the five sections analyzed. Wells 'TM6' and 'MQ1' are plotted versus their current burial depth whereas 'MD' 'KD' and 'MTN' are plotted versus stratigraphic height. The sections are aligned on the onset of the Shuram Excursion which corresponds to a sequence boundary in the outcrop sections 'MD' and 'KD'.

outcrop stratigraphy from this study (Shuram and Buah fms.) and [27] (Khufai Fm.)

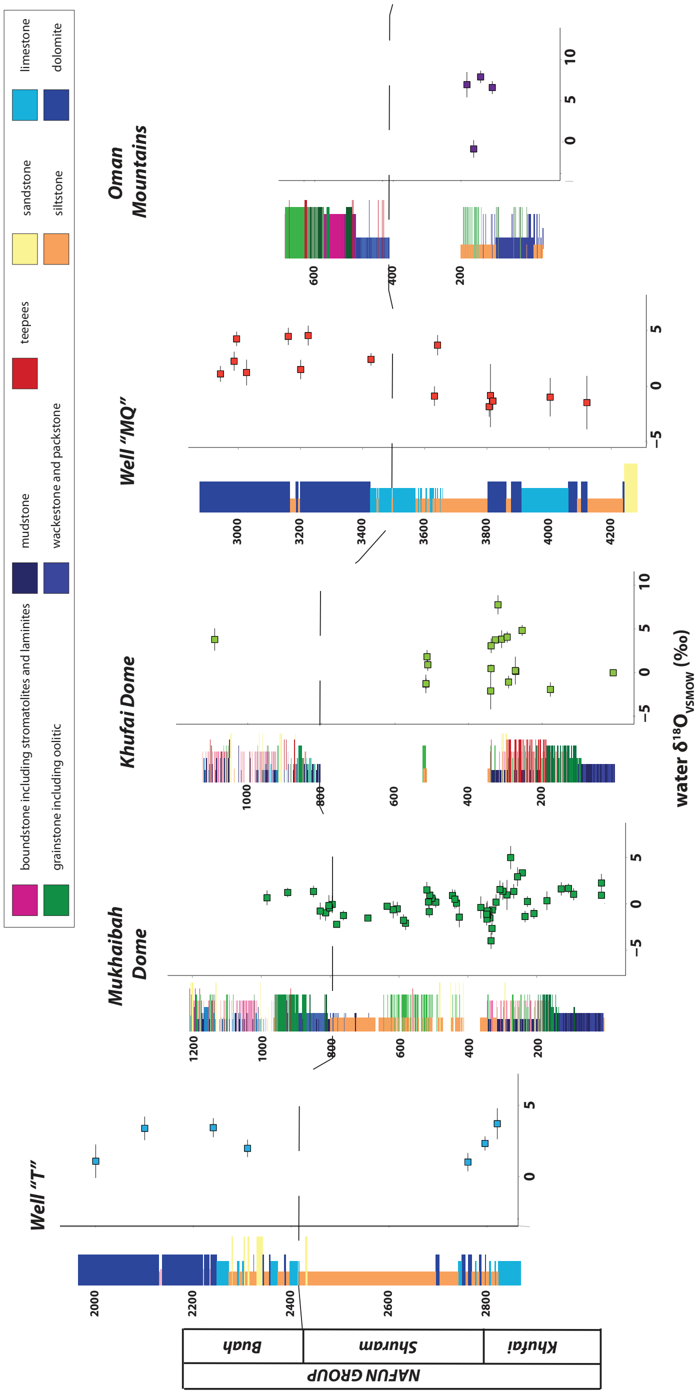

Figure 2.5: $\delta^{18}O_{water}$ of the five sections analyzed. Wells 'TM6' and 'MQ1' are plotted versus their current burial depth whereas 'MD' 'KD' and 'MTN' are plotted versus stratigraphic height. The sections are aligned on the onset of the Shuram Excursion which corresponds to a sequence boundary in the outcrop sections 'MD' and 'KD'.

outcrop stratigraphy from this study (Shuram and Buah fms.) and [27] (Khufai Fm.)

micrites showing minimal recrystallization and grain-size coarsening in thin section as well as wackestone and finely laminated stromatolites. The Type 3 samples preserve the lowest temperatures and were precipitated from fluids with $\delta^{18}O_{VSMOW}$ compositions similar to or slightly elevated relative to modern seawater (T = 38-52°C, avg. $\delta^{18}O_{water} = 0.4‰$ VSMOW)(Fig. 2.6). The more restricted lithofacies with teepee structures and evaporite mineral pseudomorphs, precipitated at similar temperatures but from fluids elevated in $\delta^{18}O$ (avg. $\delta^{18}O_{water} =$ 3‰ VSMOW).

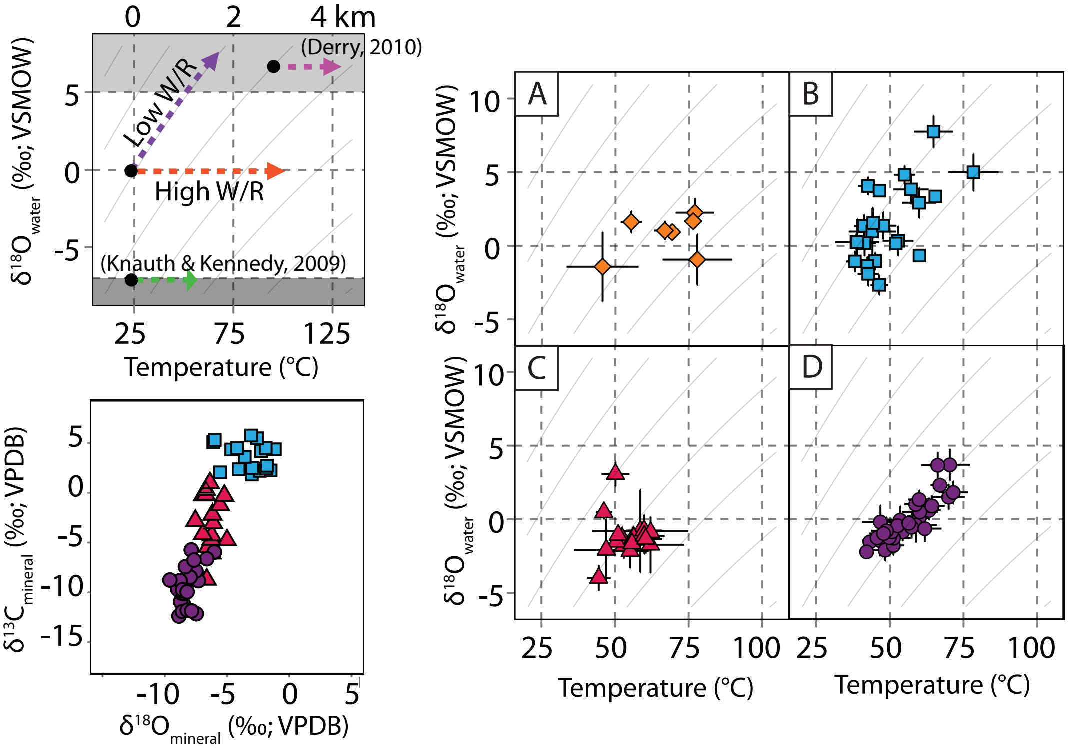

Figure 2.6: Diagenetic trends within the Shuram excursion. Clumped isotope temperature vs. calculated $\delta^{18}O_{water}$ (VSMOW) with isolines of $\delta^{18}O_{min}$ (VPDB). The lowest temperature end-members likely preserve near primary temperature-fluid compositions. A) Lower Khufai Formation samples indicating Type 1 diagenesis (high water/rock). B) Upper Khufai Formation samples from a restricted peritidal environment indicating Type 2 (low water/rock) and Type 3 diagenesis (minimal). C) Uppermost Khufai Formation samples recording the onset of the excursion indicating Type 2 and Type 3 diagenesis. D) Shuram and Buah Formation samples recording the nadir and recovery of the excursion in limestone indicating Type 2 and Type 3 diagenesis.

In the rocks recording the isotopic excursion in the uppermost Khufai, Shuram and Buah formations there is no evidence for Type 1 diagenesis (high water/rock) as previously proposed (Fig. 2.6) [5, 6]. More specifically Type 1 meteoric diagenesis would yield fluid compositions between $\sim$ -5– -7‰ and low temperatures for the most δ^{18}O depleted carbonates [6] whereas deep basinal brines driving alteration would yield enriched fluid compositions and high temperatures [5]. Dolomites preserving the onset of the isotopic excursion in the uppermost Khufai Formation generally show Type 3 diagenesis. The lowest temperatures are slightly elevated compared to samples below the sequence boundary and indicate precipitation from marine fluids estimated for ice-free conditions (T = 44-62°C, avg. $\delta^{18}O_{water}$ = -1.2‰ VSMOW). Both x-ray diffraction (XRD) and bulk trace metal data confirm a mineralogical change from dolomite to limestone at the boundary with the Shuram Formation. This mineralogical change accounts for a significant equilibrium dependent shift in $\delta^{18}O_{min}$ between the population recording the onset of the excursion and the population recording the nadir and recovery. This shift in $\delta^{18}O_{m}in$ because of mineralogy is only true if the calcite and dolomite equilibrated with the same abundant fluid (i.e., the ocean). This is confirmed because the limestone samples indicating Type 3 diagenesis precipitated from nearly identical marine fluids as the dolomite samples preserving the onset of the excursion when mineral dependent fractionation factors are used (T = 42-55°C, avg. $\delta^{18}O_{water}$ = -1.2‰ VSMOW). Type 2 diagenesis (low water/rock) is common in the samples from the nadir of the excursion (T = 56-71°C, avg. $\delta^{18}O_{water}$ = 1‰ VSMOW). This suggests the combination of low surrounding porosity in the siltstone and higher initial porosities in the oolitic grainstone allows for more fluid evolution while precipitating pore filling cements during burial.

The samples from the Oman Mountains indicate higher clumped isotope temperatures that reflect deeper burial (T = 88-152°C, avg. $\delta^{18}O_{water}$ = 8‰ VSMOW) even though the bulk δ^{13}C isotopic composition has not been altered. The clumped isotope temperatures, depleted $\delta^{18}O_{min}$ compositions and enriched $\delta^{18}O_{fluid}$ compositions indicate Type 2 diagenesis (low water/rock).

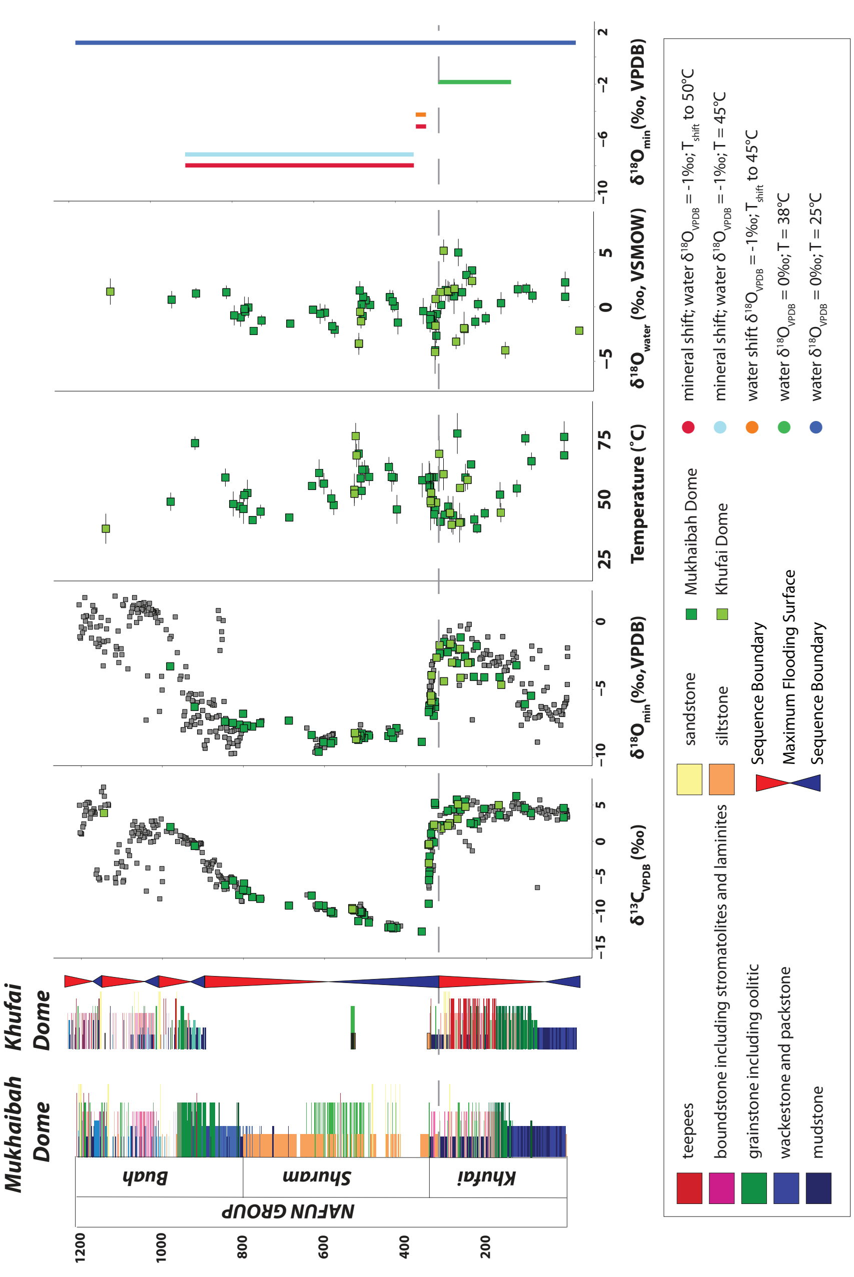

Figure 2.7: Isotopic character of the Shuram excursion. Lithofacies, $\delta^{13}C_{VPDB}$, clumped isotope temperatures, and mineral-specific calculated $\delta^{18}O_{VSMOW}$ fluid compositions for MD and KD sections. The sections are aligned using the sequence boundary near the top of the Khufai Formation.

stratigraphy and grey data from this study (Shuram and Buah fms.) and [27] (Khufai Fm.)

2.5.2 Secondary ion mass spectrometry (SIMS)

To test the possibility that a single, authigenic component that formed within the sediments is strongly controlling the bulk isotopic composition [7], SIMS analysis was completed on the different carbonate phases in two samples from the Huqf outcrop area (Fig. 2.11). Results from SIMS measurements on the two samples indicate ooids, a carbonate grain that precipitates from seawater, have very similar isotopic compositions (avg. $\delta^{13}C_{VPDB}$ = -9.5‰, -9.2‰, avg. $\delta^{18}O_{VPDB}$ =-9.2‰, -9.1‰), while authigenic porosity-occluding blocky spar cement in one sample is enriched in $\delta^{18}O_{min}$ ($\delta^{13}C_{VPDB}$ = -9.0‰, -9.1‰, $\delta^{18}O_{VPDB}$ = -7.7‰, -9.2‰). The cement enrichment is from the sample with a higher clumped isotope temperature (54°C), suggesting the cement precipitated from evolved pore fluids, likely at slightly elevated temperatures during shallow burial, however the $\delta^{13}C$ shows no modification. Early manganese-rich pink cements from that sample are more similar to the ooids ($\delta^{13}C_{VPDB}$ = -8.9‰, $\delta^{18}O_{VPDB}$ = -9.3‰). In general, the striking similarity in the SIMS measurements of ooids and cements suggests that these phases precipitated from similar fluids and temperatures (Fig. 2.11, Fig. 2.12).

2.5.3 Trace metal enrichments

The co-variation between bulk Fe and Mn concentrations and $\delta^{13}C$ isotopic composition seen in previous datasets has been proposed as additional evidence of significant post-depositional alteration (Fig. 2.7, Fig. 2.8) [5]. This line of reasoning assumes that when carbonates recrystallize during burial they often do so in the presence of reduced fluids with higher levels of Fe^{2+} and Mn^{2+} whereas carbonates precipitated from oxygenated seawater would not be enriched in reduced metals. We characterized the trace metal composition of these carbonates with a variety of bulk and micro-scale methods to test this assumption because it is clear these rocks are mixtures of carbonates and siliciclastics. Indeed $\delta^{13}C$ covaries with insoluble Al and Ti as well (Fig. 2.8). A comparison of the traditional strong acid

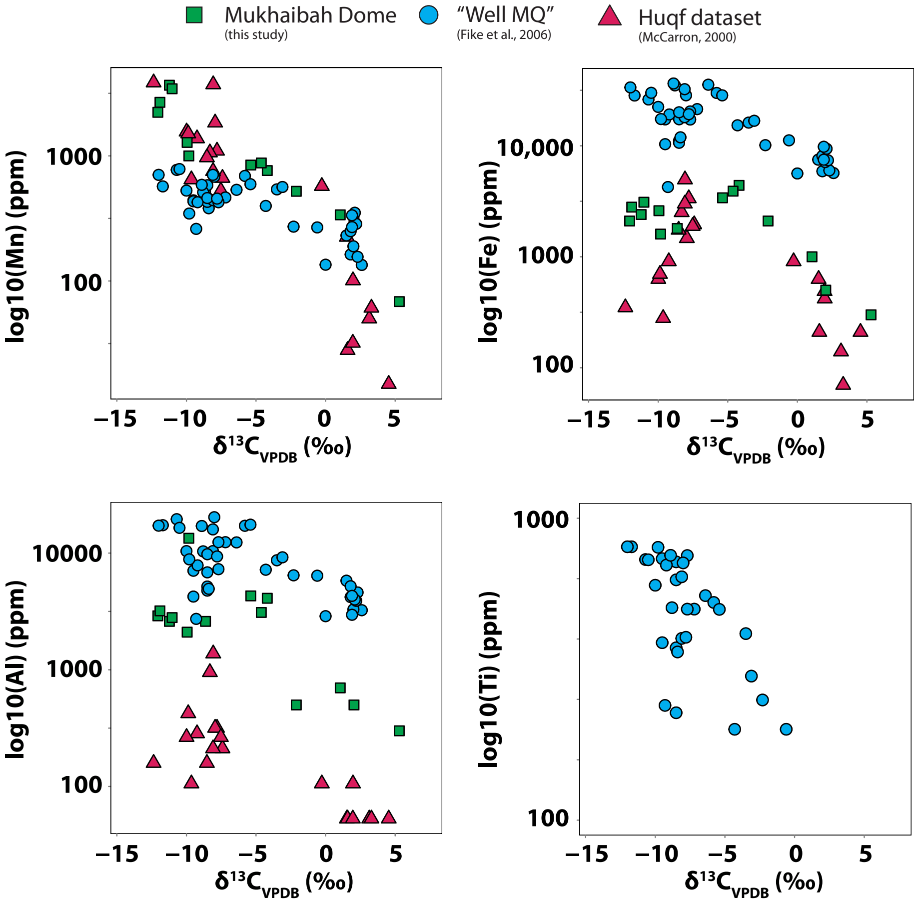

Figure 2.8: Cross plots of bulk trace metal measurements versus δ^{13}C. A–D) Log(Fe), log(Mn), log(Ti) and log(Al) versus δ^{13}C from three of the different sections analyzed. The magnitude of Fe, Al and Ti is higher for Well 'MQ' because that study dissolved both siliciclastic and carbonate cuttings in a strong acid as opposed to sampling a carbonate.

Data from this study and [56, 1]

bulk dissolution method that targets all mineral phases and an acetic dissolution that targets only the limestone in duplicate powders indicates there are distinct differences in absolute trace metal concentrations particularly for key redox metals such as iron (Fig. 2.9). Electron microprobe mapping and spot analysis of trace metal abundances can identify the important phases carrying metals including iron and manganese (Fig. 2.11). Iron it is almost completely carried in detrital phases like hematite, ilmenite, and biotite (Fig. 2.11). For example, one mixed carbonate-siliciclastic bed from the lower Shuram is composed of a significant amount of iron-rich biotite (Fig. 2.11b, i, l, Fig. 2.13). The high iron concentration in spot analyses of ooids can be attributed to small inclusions of hematite within the ooid (Fig. 2.11f, Fig. 2.12). Some authigenic hematite has coated detrital grains and mineralized ooids along surfaces likely representing depositional hiatuses to allow for the mineralization (Fig. 2.11e, h). These surfaces are often capped by intervals lean in detrital sediments but with significant secondary cement indicating faster ooid deposition.

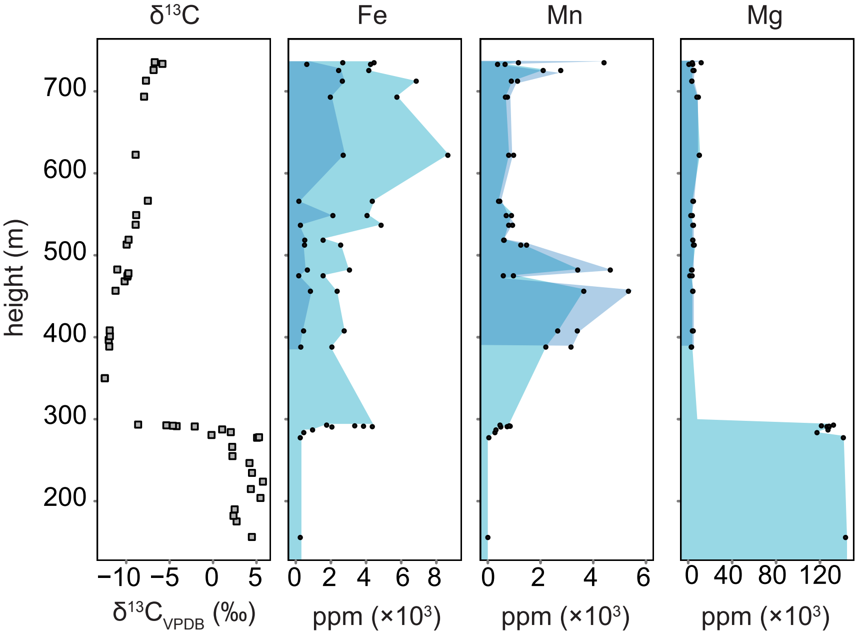

Figure 2.9: Bulk strong acid and acetic acid trace metal measurements from section MD for Fe, Mn and Mg. A strong acid dissolution (light blue) vs. an acetic acid dissolution (dark blue) targeting only the limestone indicates a significant component of the iron signal is not carried in the carbonate while most of the manganese signal is. The magnesium concentration confirms the mineralogical change to limestone.

Manganese enrichments are more complex and reinforce the petrographic and clumped isotope results that the bulk rocks are mixtures of different textures that formed at different points on the seafloor and during burial. The high trace metal values in the bulk measurements (up to 5000 ppm) can largely be attributed to reduced manganese incorporated into carbonate phases (Fig. 2.7). However, there are clear spatial differences in Mn abundance between primary grains like ooids and pore filling cements yet the δ^{13}C composition of these different phases is identical (Fig. 2.11k, l, m, Fig. 2.12). Trace manganese is also still hosted by iron oxides (visible in both EDS and electron microprobe maps)(Fig. 2.11k). The most manganese-enriched pink cements were likely precipitated early in the shallow sediments because SIMS analysis indicates these cements are more similar in isotopic compositions to ooids than the latest porosity-occluding sparry calcite cements (Fig. 2.11, 2.12).

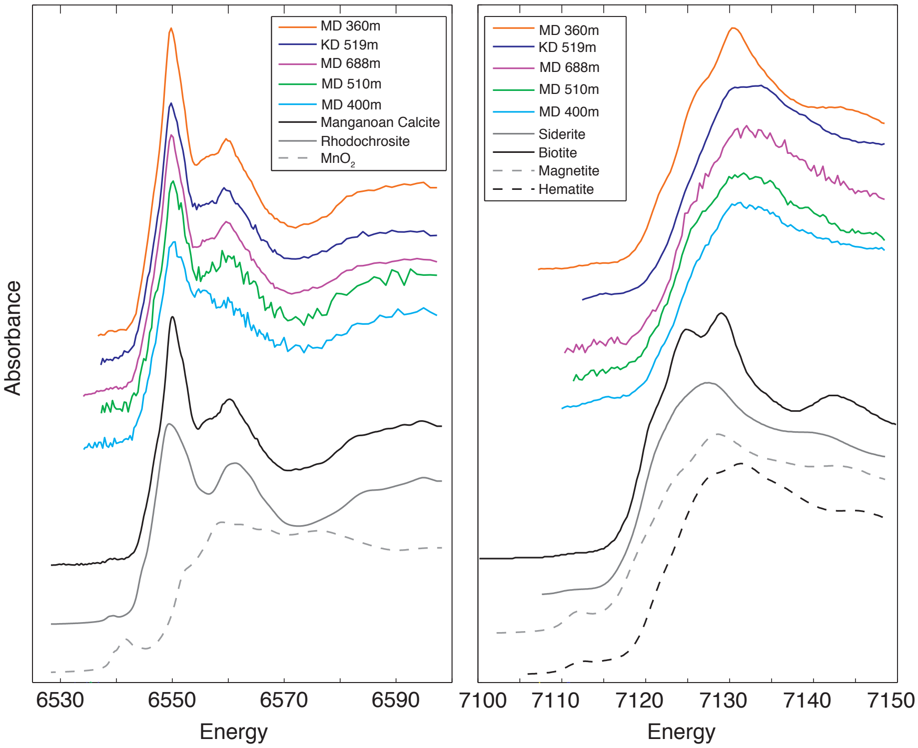

Figure 2.10: XANES spectra of samples from the Shuram Formation. XANES spectra of samples from the nadir of the excursion yield consistent results indicating the iron is found in two phases hematite and biotite while the manganese is almost completely reduced and most closely matches the spectra of manganoan calcite.

X-ray absorption near-edge spectroscopy (XANES) confirms the ICP and electron microprobe results, indicating iron is mostly oxidized Fe^{3+} in hematite or is mixed valence iron in biotite, whereas manganese is mostly reduced Mn^{2+} and is most similar to the spectra of a manganoan calcite standard (Fig. 2.10). The manganese and iron results together with a lack of pyrite imply minimal anaerobic respiration occurred. Studies have suggested producing an excursion of such magnitude would deplete available oxidants contradict the evidence that there were abundant available oxidants in the Huqf outcrop area in the form of iron oxides that were only partially reduced [4].

2.6 Discussion

We suggest the combined bulk carbonate clumped isotope thermometry and micro-scale SIMS analysis is the δ^{13}C composition of these rocks reflects time-varying trends in marine DIC and clumped isotope temperatures of samples indicating Type 3 diagenesis reflect near primary temperatures. Support for this includes $\delta^{18}O_{VSMOW}$ fluid compositions, which shift from evaporitic compositions in the peritidal carbonates of the Upper Khufai Formation ($\sim$ 0–2‰) to marine ice-free compositions ($\sim$ -1.2‰) at the onset of the excursion. The shift in fluid composition and concurrent temperature increase occurs above a sequence boundary in rocks with sedimentary characteristics indicating deposition during a transgression (Fig. 2.7) [41]. The samples in the Shuram and Buah formations preserve similar fluids and temperatures to the dolomites preserving the onset, thus the second shift in $\delta^{18}O_{min}$ is entirely due to a mineralogical change to limestone (Fig. 2.7). Both the isotopic character and sedimentology of the Johnnie Formation, Death Valley, another Ediacaran-aged formation with a similar magnitude negative excursion, suggest a transgression coincident with the isotopic excursion [57, 58]. Additionally, a mineralogical shift from dolomite to limestone also occurs in the Johnnie, Wonoka and Doushantuo formations at a similar stratigraphic height in the excursion (above $\sim$ -6‰) [13, 15, 58]. A major reason the δ^{13}C and δ^{18}O co-variation is observed globally is because of the isotopic difference between calcite-water and dolomite-water equilibrium fractionation reinforcing that this excursion is a primary isotopic signal.

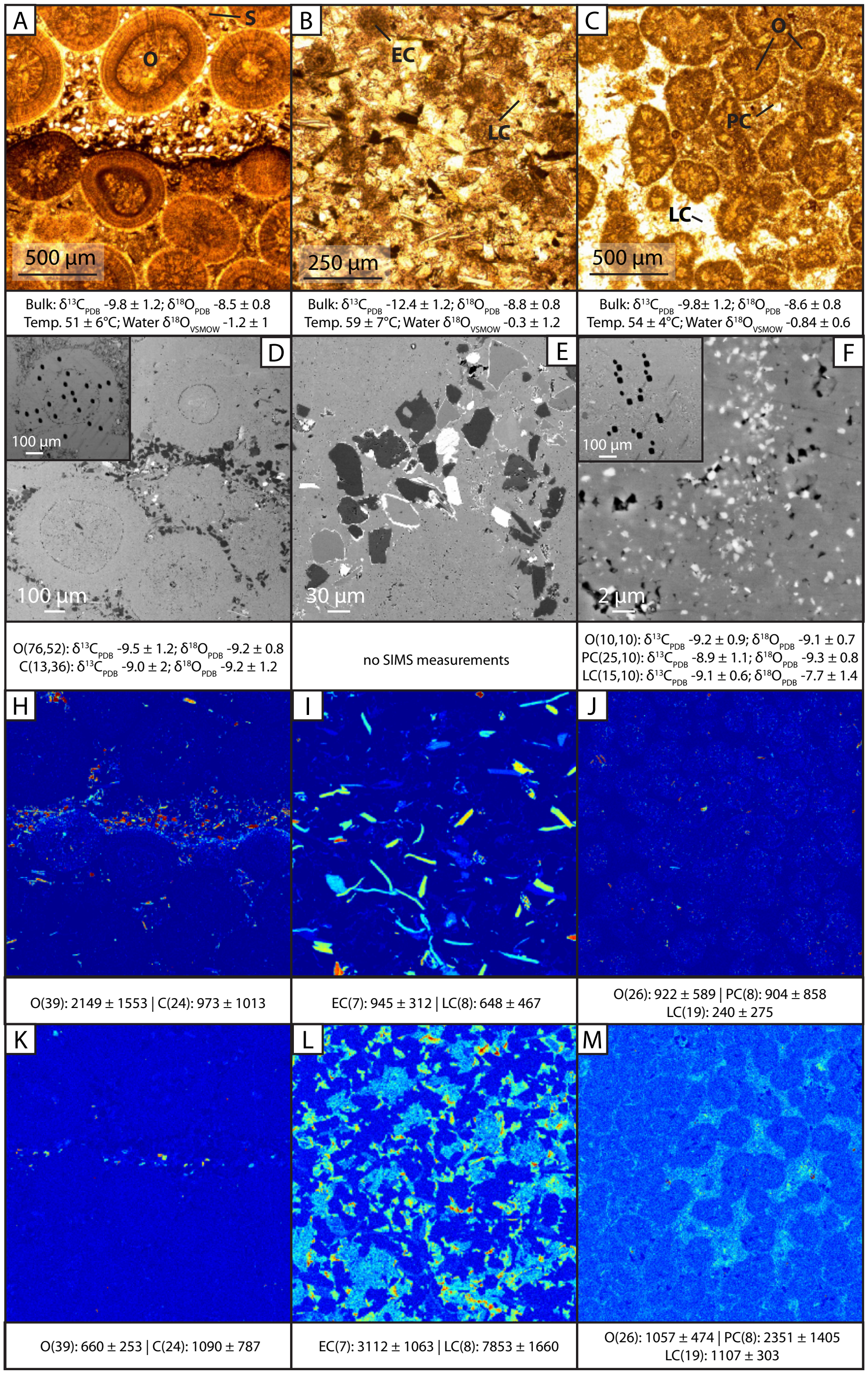

Figure 2.11: Caption on following page

Figure 2.11: In situ isotopic (SIMS) and trace metal (electron microprobe) variations. A–C) Thin-section photomicrographs of three representative fabrics from the nadir of the excursion with ooids (O), sediment (S), early and late cements (EC and LC), pink cements (PC), D–F) SEM images highlighting ooids with abundant accessory minerals infilling around the grains and in F finely disseminated iron oxides within the ooids. The insets show SIMS spot analyses across ooids. SIMS measurements of ooids and cement are reported below the image with 1 SD, H–J) Electron microprobe elemental maps of iron in the three samples shown in A–C. The high intensities in H are dominantly iron oxides whereas in I they are dominantly biotite grains. Spot analyses of Fe concentrations in carbonate are reported below each image with 1 SD. K–M) Electron microprobe elemental maps of manganese. The high intensity areas in K is manganese incorporated into oxides whereas in L and M the high intensity areas are in authigenic carbonate cements. Spot analyses of Mn concentrations in carbonate are reported below each image with 1 SD.

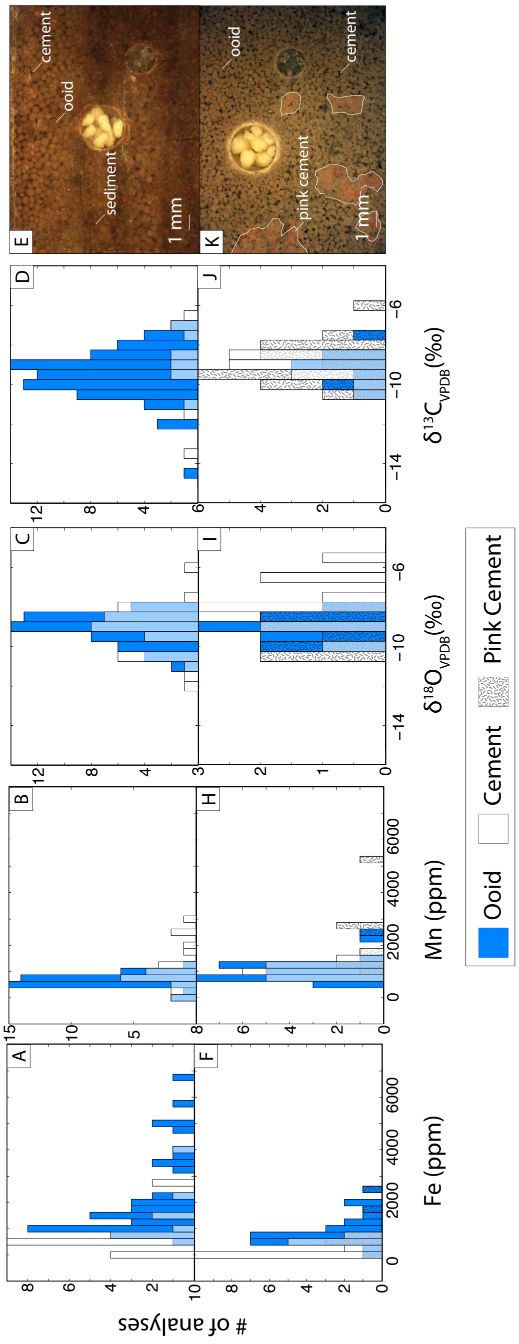

Figure 2.12: Histograms of in-situ data for two samples from the Shuram Formation. A & F) Spot analyses of iron (ppm) on ooids and two cement types—clear blocky cements and pink microcrystalline cements. B & G) Spot analyses of manganese (ppm). C & H) Spot analyses of $\delta^{13}C_{VPDB}$. d and i, spot analyses of $\delta^{18}O_{VPDB}$. E & J) Images of each sample showing ooids, two types of cements and imbedded standards (± 1‰ SD).

The most important conclusion from our metal characterization is that bulk trace metal measurements of carbonates should not be interpreted as a simple metric of diagenesis. The spatial pattern in trace metal enrichments also does not support a model where these rocks have been isotopically homogenized during a fluid flushing diagenetic event as proposed by others [5, 6]. Instead, it is clear that a defining character of the isotopic excursion preserved in the Khufai, Shuram and Buah formations is the coincident delivery of a large volume of fine-grained (avg. 25 μm), poorly weathered detrital material to the shallow marine environment (Fig. 2.13, Fig. 2.8). Characterization of the detrital component of the Rainstorm Member of the Johnnie Formation in Death Valley indicates similarly diverse detrital minerals with an identical average grain size (Fig. 2.13) [59]. In both sections minerals found include biotite, muscovite, plagioclase, potassium feldspar, rutile, anatase, zircon, ilmenite, hematite, and quartz. Our combined results suggest this large volume of poorly weathered, silt-sized material is being introduced in conjunction with a transgression in both locations. The detrital component of both the Shuram and Johnnie formations fits many characteristics of loess—windblown deposits—including the consistent, fine grain size, abundant poorly weather minerals like muscovite and biotite as well as abundant heavy minerals (Fig. 2.11, Fig. 2.13).

The combined results of the sedimentology, sequence stratigraphy, clumped isotope thermometry, SIMS, and the trace metal analyses suggest a series of concurrent events at the onset of the Shuram Excursion. Above the sequence boundary, along with the rapid decline in $\delta^{13}C_{min}$, there is a coincident temperature increase, a shift to marine ice-free seawater compositions, and the introduction of poorly weathered, fine detrital material. The Ediacaran-aged Shuram Excursion is not the only large negative carbon isotope excursion to punctuate the Neoproterozoic rock record. Extreme negative carbon isotopic excursions are documented preceding and post-dating both the Sturtian and Marinoan glacial deposits [60, 61]. Although the Shuram Excursion and the other Ediacaran excursions correlated with it lack precise age constraints it is possible that this excursion could be

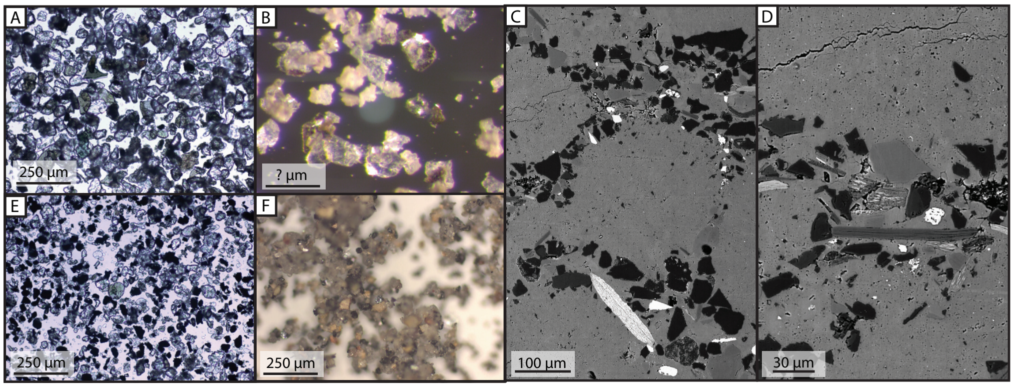

Figure 2.13: Detrital fraction of the Shuram (A-D) and Johnnie Formations (E–F). A & E) Wet grain mount under 10X magnification with visible biotite and muscovite grains. Iron oxides are much more abundant in the sample from the Johnnie Formation. B & F) Dry grain mount with quartz, muscovite, biotite, iron oxides and feldspars visible. The coarser grains in a fine sandstone from the Shuram Formation include poorly weathered micas. C & D) SEM images of iron-rich biotite grains within the detrital sediments filling in around the ooids.

linked to a glaciation [60, 11], while others have suggested the Shuram Excursion is likely younger than any glacial deposits [22, 20]. The potential remains that similarities in the global conditions driving these large negative excursions have a climatic component that can be directly tied to interglacial periods. A model that fits much of the observed data of the Shuram Excursion is that it is related to a deglaciation resulting in a temperature increase, change to ice-free $\delta^{18}O_{seawater}$ values, a transgression and the delivery of a large volume of new exposed glacially derived loess. The character of loess associated with the Pleistocene glaciations is similar to the silts of the Shuram and Johnnie Formations [62, 63, 64]. Other sections preserving the negative excursion appear to be similarly dominated by thick red siltstones and could benefit from further study of the detrital makeup (i.e., Wonoka Formation [13]). While the correlated $\delta^{13}C$ decline, transgression, temperature increase, fluid change and increased detrital input do not necessarily deglaciation, we think it could provide the necessary mechanism to affect all of these stratigraphic and geochemical parameters simultaneously.

2.7 Conclusions

Multiple proposed mechanisms for the large negative carbon isotope excursions common in Neoproterozoic strata have relied on either open-system diagenesis involving a non-seawater-like fluid or authigenic precipitates with a depleted isotopic composition [5, 6, 7]. We find lots of evidence for diagenesis within the Nafun Group, however none of it is temporally associated with the δ^{13}C excursion. Neither the carbonate clumped isotope thermometry or micro-scale SIMS analysis supports the previously proposed diagenetic mechanisms. Instead the data suggests many of the carbonates are well preserved enough to not only record secular changes in marine DIC but also a transgression and temperature increase and an input of fine, unweathered detrital material, potentially loess. A mineralogical change from dolomite to limestone appears to be global in nature and accounts for a component of the correlation previously observed between δ^{13}C and δ^{18}O. If these temperatures recording precipitation from seawater-like fluids are only slightly modified from sea surface temperatures, elevated temperatures for periods of the Neoproterozoic could have profound implications for our understanding of the biological and climatic events preceding the Cambrian explosion.

2.8 Acknowledgements

We would like to thank Nami Kitchen, Joel Hurowitz, Chi Ma, and Yunbin Guan for assistance with analytical measurements. Sam Webb and Jena Johnson helped with the XANES measurements at SLAC and provided standard data. We would also like to thank Magali Bonifaci for providing the high-temperature dolomite calibration dataset used as part of our calibration line. A National Science Foundation Graduate Research Fellowship was provided to K. Bergmann. Funding for analytical measurements was provided by the Agouron Institute and NASA Astrobiology Institute.

References

[1] D.A. Fike, J.P. Grotzinger, L.M. Pratt, and R.E. Summons. Oxidation of the Ediacaran ocean. *Nature*, 444(7120):744–747, 2006.

[2] J.P. Grotzinger, D.A. Fike, and W.W. Fischer. Enigmatic origin of the largest-known carbon isotope excursion in Earth's history. *Nature Geoscience*, 4(5):285–292, 2011.

[3] D.H. Rothman, J.M. Hayes, and R.E. Summons. Dynamics of the Neoproterozoic carbon cycle. *Proceedings of the National Academy of Sciences of the United States of America*, 100(14):8124–8129, 2003.

[4] T.F. Bristow and M.J. Kennedy. Carbon isotope excursions and the oxidant budget of the Ediacaran atmosphere and ocean. *Geology*, 36(11):863–866, 2008.

[5] L.A. Derry. A burial diagenesis origin for the Ediacaran Shuram-Wonoka carbon isotope anomaly. *Earth and Planetary Science Letters*, 294(1-2):152–162, 2010.

[6] L.P. Knauth and M.J. Kennedy. The late Precambrian greening of the Earth. *Nature*, 460(7256):728–732, 2009.

[7] D.P. Schrag, J.A. Higgins, F.A. Macdonald, and D.T. Johnston. Authigenic carbonate and the history of the global carbon cycle. *Science*, 339(6119):540–543, 2013.

[8] P.K. Swart and G. Eberli. The nature of the delta C-13 of periplatform sediments: Implications for stratigraphy and the global carbon cycle. *Sedimentary Geology*, 175(1-4):115–129, 2005.

[9] P.A. Cohen, A. Bradley, A.H. Knoll, J.P. Grotzinger, S. Jensen, J. Abelson, K. Hand, G. Love, J. Metz, N. Mcloughlin, P. Meister, R. Shepard, M. Tice, and J.P. Wilson. Tubular compression fossils from the Ediacaran Nama Group, Namibia. *Journal of Paleontology*, 83(1):110–122, 2009.

[10] C.V. Rose, N.L. Swanson-Hysell, J.M. Husson, L.N. Poppick, J.M. Cottle, B. Schoene, and A.C. Maloof. Constraints on the origin and relative timing of the Trezona delta C-13 anomaly below the end-Cryogenian glaciation. *Earth and Planetary Science Letters*, 319:241–250, 2012.

[11] G.P. Halverson, B.P. Wade, M.T. Hurtgen, and K.M. Barovich. Neoproterozoic chemostratigraphy. *Precambrian Research*, 182(4):337–350, 2010.

[12] S.J. Burns and A. Matter. Carbon isotopic record of the latest Proterozoic from Oman. *Eclogae Geologicae Helvetiae*, 86(2):595–607, 1993.

[13] C.R. Calver. Isotope stratigraphy of the Ediacaran (Neoproterozoic III) of the Adelaide Rift Complex, Australia, and the overprint of water column stratification. *Precambrian Research*, 100(1-3):121–150, 2000.

[14] G.Q. Jiang, A.J. Kaufman, N. Christie-Blick, S.H. Zhang, and H.C. Wu. Carbon isotope variability across the Ediacaran Yangtze platform in South China: Implications for a large surface-to-deep ocean delta C-13 gradient. *Earth and Planetary Science Letters*, 261(1-2):303–320, 2007.

[15] K.A. McFadden, J. Huang, X.L. Chu, G.Q. Jiang, A.J. Kaufman, C.M. Zhou, X.L. Yuan, and S.H. Xiao. Pulsed oxidation and biological evolution in the Ediacaran Doushantuo Formation. *Proceedings of the National Academy of Sciences of the United States of America*, 105(9):3197–3202, 2008.

[16] F.A. Corsetti and A.J. Kaufman. Stratigraphic investigations of carbon isotope anomalies and Neoproterozoic ice ages in Death Valley, California. *Geological Society of America Bulletin*, 115(8):916–932, 2003.

[17] C. Verdel, B.P. Wernicke, and S.A. Bowring. The Shuram and subsequent Ediacaran carbon isotope excursions from southwest Laurentia, and implications for environmental stability during the metazoan radiation. *Geological Society of America Bulletin*, 123(7/8):1539–1559, 2011.

[18] V.A. Melezhik, B.G. Pokrovsky, A.E. Fallick, A.B. Kuznetsov, and M.I. Bujakaite. Constraints on Sr-87/Sr-86 of Late Ediacaran seawater: insight from Siberian high-Sr limestones. *Journal of the Geological Society*, 166:183–191, 2009.

[19] B.Z. Saylor, A.J. Kaufman, J.P. Grotzinger, and F. Urban. A composite reference section for terminal Proterozoic strata of southern Namibia. *Journal of Sedimentary Research*, 68(6):1223–1235, 1998.

[20] A.R. Prave, R.A. Strachan, and A.E. Fallick. Global C cycle perturbations recorded in marbles: a record of Neoproterozoic Earth history within the Dalradian succession of the Shetland Islands, Scotland. *Journal of the Geological Society*, 166:129–135, 2009.

[21] V.A. Melezhik, D. Roberts, A.E. Fallick, and I.M. Gorokhov. The Shuram-Wonoka event recorded in a high-grade metamorphic terrane: Insight from the Scandinavian Caledonides. *Geological Magazine*, 145(2):161–172, 2008.

[22] D. Condon, M.Y. Zhu, S. Bowring, W. Wang, A.H. Yang, and Y.G. Jin. U-Pb ages from the Neoproterozoic Doushantuo Formation, China. *Science*, 308(5718):95–98, 2005.

[23] J.G. Gehling and M.L. Droser. Ediacaran stratigraphy and the biota of the Adelaide Geosyncline, South Australia. *Episodes*, 35(1):236–246, 2012.

[24] J.W. Hagadorn, C.M. Fedo, and B.M. Waggoner. Early Cambrian Ediacaran-type fossils from California. *Journal of Paleontology*, 74(4):731–740, 2000.

[25] L.R. Kump. Interpreting carbon-isotope excursions - strangelove oceans. *Geology*, 19(4):299–302, 1991.

[26] D.T. Johnston, F. A. Macdonald, B. C. Gill, P. F. Hoffman, and D. P. Schrag. Uncovering the Neoproterozoic carbon cycle. *Nature*, 483(7389):320–324, 2012.

[27] M. Osburn. *Isotopic proxies for microbial and environmental change: Insights from Compound-Specific hydrogen Isotopes the and Ediacaran Khufai Formation.* Ph.D. thesis, 2013.

[28] D.A. Fike and J.P. Grotzinger. A paired sulfate-pyrite delta S-34 approach to understanding the evolution of the Ediacaran-Cambrian sulfur cycle. *Geochimica Et Cosmochimica Acta*, 72(11):2636–2648, 2008.

[29] R.K. Given and K.C. Lohmann. Isotopic evidence for the early meteoric diagenesis of the reef facies, Permian Reef Complex of West Texas and New Mexico. *Journal of Sedimentary Petrology*, 56(2):183–193, 1986.

[30] J.L. Banner and G.N. Hanson. Calculation of simultaneous isotopic and trace-element variations during water-rock interaction with applications to carbonate diagenesis. *Geochimica Et Cosmochimica Acta*, 54(11):3123–3137, 1990.

[31] J. Zachos, M. Pagani, L. Sloan, E. Thomas, and K. Billups. Trends, rhythms, and aberrations in global climate 65 Ma to present. *Science*, 292(5517):686–693, 2001.

[32] P.J. Brenchley, G.A. Carden, L. Hints, D. Kaljo, J.D. Marshall, T. Martma, T. Meidla, and J. Nolvak. High-resolution stable isotope stratigraphy of upper Ordovician sequences: Constraints on the timing of bioevents and environmental changes associated with mass extinction and glaciation. *Geological Society of America Bulletin*, 115(1):89–104, 2003.

[33] A.L. Cohen and M. Holcomb. Why corals care about ocean acidification: Uncovering the mechanism. *Oceanography*, 22(4):118–127, 2009.

[34] E. Le Guerroue, P.A. Allen, and A. Cozzi. Chemostratigraphic and sedimentological framework of the largest negative carbon isotopic excursion in Earth history: The Neoproterozoic Shuram Formation (Nafun Group, Oman). *Precambrian Research*, 146(1-2):68–92, 2006.

[35] S.T. Kim and J.R. Oneil. Equilibrium and nonequilibrium oxygen isotope effects in synthetic carbonates. *Geochimica Et Cosmochimica Acta*, 61(16):3461–3475, 1997.

[36] C. Vasconcelos, J.A. McKenzie, R. Warthmann, and S.M. Bernasconi. Calibration of the delta O-18 paleothermometer for dolomite precipitated in microbial cultures and natural environments. *Geology*, 33(4):317–320, 2005.

[37] J.M. Ferry, B.H. Passey, C. Vasconcelos, and J.M. Eiler. Formation of dolomite at 40-80 degrees c in the Latemar carbonate buildup, dolomites, Italy, from clumped isotope thermometry. *Geology*, 39(6):571–574, 2011.

[38] E.M. Swanson, B.P. Wernicke, J.M. Eiler, and S. Losh. Temperatures and fluids on faults based on carbonate clumped-isotope thermometry. *American Journal of Science*, 312(1):1–21, 2012.

[39] S.A. Bowring, J.P. Grotzinger, D.J. Condon, J. Ramezani, M.J. Newall, and P.A. Allen. Geochronologic constraints on the chronostratigraphic framework of the Neoproterozoic Huqf Supergroup, Sultanate of Oman. *American Journal of Science*, 307(10):1097–1145, 2007.

[40] E. Le Guerroue, P.A. Allen, and A. Cozzi. Parasequence development in the Ediacaran Shuram Formation (Nafun Group, Oman): high-resolution stratigraphic test for primary origin of negative carbon isotopic ratios. *Basin Research*, 18(2):205–219, 2006.

[41] M. Osburn, J. Grotzinger, and K. Bergmann. Facies, stratigraphy, and evolution of a Middle-Ediacaran-age carbonate ramp: Khufai Formation, Sultanate of Oman. *AAPG Bulletin*, inpress.

[42] J.P. Grotzinger. Evolution of Early Proterozoic passive-margin carbonate platform, Rocknest Formation, Wopmay Orogen, Northwest-Territories, Canada. *Journal of Sedimentary Petrology*, 56(6):831–847, 1986.

[43] A. Cozzi, P.A. Allen, and J.P. Grotzinger. Understanding carbonate ramp dynamics using delta C-13 profiles: examples from the Neoproterozoic Buah Formation of Oman. *Terra Nova*, 16(2):62–67, 2004.

[44] A. Cozzi, J.P. Grotzinger, and P.A. Allen. Evolution of a terminal Neoproterozoic carbonate ramp system (Buah Formation, Sultanate of Oman): Effects of basement paleotopography. *Geological Society of America Bulletin*, 116(11-12):1367–1384, 2004.

[45] K.W. Huntington, J.M. Eiler, H.P. Affek, W. Guo, M. Bonifacie, L.Y. Yeung, N. Thiagarajan, B. Passey, A. Tripati, M. Daeron, and R. Came. Methods and limitations of 'clumped' CO2 isotope (Delta(47)) analysis by gas-source isotope ratio mass spectrometry. *Journal of Mass Spectrometry*, 44(9):1318–1329, 2009.

[46] B.H. Passey, N.E. Levin, T.E. Cerling, F.H. Brown, and J.M. Eiler. High-temperature environments of human evolution in East Africa based on bond ordering in paleosol carbonates. *Proceedings of the National Academy of Sciences of the United States of America*, 107(25):11245–11249, 2010.

[47] K.J. Dennis, H.P. Affek, B.H. Passey, D.P. Schrag, and J.M. Eiler. Defining an absolute reference frame for 'clumped' isotope studies of CO2. *Geochimica Et Cosmochimica Acta*, 75(22):7117–7131, 2011.

[48] G.A. Henkes, B. Passey, A.D. WaNamaker, E.L. Grossman, W.G. Ambrose, and M.L. Carroll. Carbonate clumped isotope compositions of modern

marine mollusk and brachiopod shells. *Geochimica Et Cosmochimica Acta*, 106(1):307–325, 2013.

[49] M. Bonifaci and J. Eiler. High temperature dolomite calibration. inpress.

[50] P. Ghosh, J. Adkins, H. Affek, B. Balta, W.F. Guo, E.A. Schauble, D. Schrag, and J.M. Eller. C-13-O-18 bonds in carbonate minerals: A new kind of paleothermometer. *Geochimica Et Cosmochimica Acta*, 70(6):1439–1456, 2006.

[51] J. Rosenbaum and S.M.F. Sheppard. An isotopic study of siderites, dolomites and ankerites at high-temperatures. *Geochimica Et Cosmochimica Acta*, 50(6):1147–1150, 1986.

[52] P.K. Swart, S.J. Burns, and J.J. Leder. Fractionation of the stable isotopes of oxygen and carbon in carbon-dioxide during the reaction of calcite with phosphoric-acid as a function of temperature and technique. *Chemical Geology*, 86(2):89–96, 1991.

[53] A. Matthews and A. Katz. Oxygen isotope fractionation during dolomitization of calcium-carbonate. *Geochimica Et Cosmochimica Acta*, 41(10):1431–1438, 1977.

[54] M. Schmidt, S. Xeflide, R. Botz, and S. Mann. Oxygen isotope fractionation during synthesis of CaMg-carbonate and implications for sedimentary dolomite formation. *Geochimica Et Cosmochimica Acta*, 69(19):4665–4674, 2005.

[55] C.B. Tennant and R.W. Berger. X-ray determination of dolomite-calcite ratio of a carbonate rock. *American Mineralogist*, 42(1-2):23–29, 1957.

[56] G.M.E. McCarron. *The sedimentology and chemostratigraphy of the Nafun Group, Huqf Supergroup, Oman.* Ph.D. thesis, 2000.

[57] K.D. Bergmann, R.A. Zentmyer, and W.W. Fischer. The stratigraphic expression of a large negative carbon isotope excursion from the Ediacaran Johnnie Formation, Death Valley. *Precambrian Research*, 188:45–56, 2011.

[58] C. Summa. *Sedimentologic, stratigraphic, and tectonic controls of a mixed carbonate-siliciclastic succession: Neoproterozoic Johnnie Formation, southeast California*. Ph.D. thesis, 1993.

[59] K. Bergmann, J.P. Grotzinger, and W.W. Fischer. Biological influence on seafloor carbonate precipitation. *Palaios*, 28(2):99–115, 2013.

[60] G.P. Halverson, P.F. Hoffman, D.P. Schrag, A.C. Maloof, and A.H.N. Rice. Toward a Neoproterozoic composite carbon-isotope record. *Geological Society of America Bulletin*, 117(9-10):1181–1207, 2005.

[61] P.F. Hoffman, A.J. Kaufman, G.P. Halverson, and D.P. Schrag. A Neoproterozoic snowball Earth. *Science*, 281(5381):1342–1346, 1998.

[62] K. Pye. The nature, origin and accumulation of loess. *Quaternary Science Reviews*, 14(7-8):653–667, 1995.

[63] N.R. Winspear and K. Pye. Textural, geochemical and mineralogical evidence for the origin of Peoria loess in central and southern Nebraska, USA. *Earth Surface Processes and Landforms*, 20(8):735–745, 1995.

[64] J.S. Wright. ”desert” loess versus ”glacial” loess: quartz silt formation, source areas and sediment pathways in the formation of loess deposits. *Geomorphology*, 36(3-4):231–256, 2001.